UC Berkeley

UC Berkeley Previously Published Works

Title

Modification of Salmonella Lipopolysaccharides Prevents the Outer Membrane Penetration of Novobiocin

Permalink

https://escholarship.org/uc/item/8ph553sd

Journal

Biophysical Journal, 109(12)

ISSN

0006-3495

Authors

Nobre, Thatyane M
Martynowycz, Michael W
Andreev, Konstantin
et al.

Publication Date

2015-12-01

DOI

10.1016/j.bpj.2015.10.013

Peer reviewed

eScholarship.org Powered by the California Digital Library
University of California

Article

Modification of *Salmonella* Lipopolysaccharides Prevents the Outer Membrane Penetration of Novobiocin

Thatyane M. Nobre,[1,2,*] Michael W. Martynowycz,[3,4] Konstantin Andreev,[3] Ivan Kuzmenko,[4] Hiroshi Nikaido,[1] and David Gidalevitz[3,*]

[1]Department of Molecular and Cell Biology, University of California at Berkeley, Berkeley, California; [2]Molecular Foundry, Lawrence Berkeley National Laboratory, Berkeley, California; [3]Center for Molecular Study of Condensed Soft Matter and Department of Physics, Illinois Institute of Technology, Chicago, Illinois; and [4]X-ray Science Division, Advanced Photon Source, Argonne National Laboratory, Lemont, Illinois

ABSTRACT Small hydrophilic antibiotics traverse the outer membrane of Gram-negative bacteria through porin channels. Large lipophilic agents traverse the outer membrane through its bilayer, containing a majority of lipopolysaccharides in its outer leaflet. Genes controlled by the two-component regulatory system PhoPQ modify lipopolysaccharides. We isolate lipopolysaccharides from isogenic mutants of *Salmonella* sp., one lacking the modification, the other fully modified. These lipopolysaccharides were reconstituted as monolayers at the air-water interface, and their properties, as well as their interaction with a large lipophilic drug, novobiocin, was studied. X-ray reflectivity showed that the drug penetrated the monolayer of the unmodified lipopolysaccharides reaching the hydrophobic region, but was prevented from this penetration into the modified lipopolysaccharides. Results correlate with behavior of bacterial cells, which become resistant to antibiotics after PhoPQ-regulated modifications. Grazing incidence x-ray diffraction showed that novobiocin produced a striking increase in crystalline coherence length, and the size of the near-crystalline domains.

INTRODUCTION

Gram-negative bacteria possess an asymmetric double-layered outer membrane, with its external leaflet composed almost exclusively of lipopolysaccharides (LPS) (1). Although antimicrobial agents that are small and hydrophilic can traverse this membrane through porin channels (1), agents that are large and/or lipophilic cannot permeate through this route (2,3), and thus they must use the LPS-phospholipid asymmetric bilayer region for permeation (1). This bilayer serves as an unusually low permeability barrier (4,5) because of the structure of the LPS, which serves as a robust barrier for the cell's protection from external chemicals, including antibiotics (1). Their intrinsic lack of susceptibility to many lipophilic antibiotics is related to the low permeability of their outer membrane bilayer (6). LPS molecules are typically composed of a highly hydrophobic anchor, lipid A, which can have up to seven saturated fatty acids per molecule, a short basal core oligosaccharide containing several acidic groups, a short peripheral core oligosaccharide, and finally an O antigen consisting of relatively long polysaccharides (1,4). That the LPS leaflet acts as a major permeability barrier was shown by the observation that mutants in LPS biosynthesis resulting in the defective basal core, often called deep rough mutants, become hyper susceptible to large lipophilic antibiotics such as novobiocin and macrolides (6). In contrast, mutants with a complete R core or mutants with a core deficient only in galactose or *N*-acetyl glucosamine result in an essentially unaltered barrier (6).

The molecular mechanisms involved in the highly effective barrier property of LPS leaflet undoubtedly involves the presence of 5–7 saturated fatty acyl chains all connected to a single headgroup as mentioned earlier; this induces a gel-like state of very low fluidity at the outer membrane surface (1). This barrier also involves a strong interaction between the neighboring LPS molecules: LPS contains many anionic groups close to the membrane surface, due to, typically, two monophosphate groups in the lipid A portion of LPS, carboxyl groups in the 2-keto-3-deoxyoctulosonate (KDO) residues, and phosphate groups on the heptose residues all within the basal core oligosaccharide. Thus, the bridging of negative charges by a bivalent cation such as Mg^{2+} or Ca^{2+} could be a major factor leading to a strong lateral interaction between LPS molecules. This concept is supported by the observation that chelators such as EDTA that remove bivalent cations, or polycationic agents that compete with bivalent cations increase profoundly the susceptibility of Gram-negative bacteria toward large, lipophilic agents, without affecting their susceptibility to small, hydrophilic antibiotics (7). Finally, hydrogen bonds between neighboring LPS molecules might also strengthen the lateral interaction. The LPS of *Salmonella enterica* serovar Typhimurium undergoes extensive remodeling through the PhoPQ two-component system in response to the nature of the environment (8). When salmonellae enter the phagosomes of mammalian

Submitted May 18, 2015, and accepted for publication October 8, 2015.

*Correspondence: gidalevitz@iit.edu or thatty@ursa.ifsc.usp.br

Thatyane M. Nobre and Michael W. Martynowycz contributed equally to this work.

Editor: Francesca Marassi.

© 2015 by the Biophysical Society

0006-3495/15/12/2537/9

http://dx.doi.org/10.1016/j.bpj.2015.10.013

host cells, PhoPQ pathway increases transcription of the genes responsible for LPS modification, such as *pagP* that adds an extra palmitoyl group, *pmrAB* that adds a positively charged aminoarabinose to the lipid A headgroup, and *lpxO* that adds a 2-hydroxyl group to one of the fatty acid residues. These modifications create an outer membrane (OM) that is more resistant to the cationic antimicrobial peptides of the host by decreasing the net negative charges of LPS and increasing the lateral interactions between neighboring LPS molecules. They also create a more robust permeability barrier against large, lipophilic agents such as novobiocin, rifampin, erythromycin, and ethidium bromide (9).

Langmuir monolayers mimic half of a cellular membrane, and allow for precise control over the composition and physical state of a membrane, all while using a very small amount of material. Due to their planar configuration, Langmuir monolayers are advantageous for studying complex molecules, like LPS, because it is not always possible to build asymmetrical bilayer systems with these types of materials. Additionally, the use of Langmuir monolayers can be coupled with high precision synchrotron studies done by using a liquid surface spectrometer, allowing for physical characterization at a molecular level. In this study, we examine permeability of *Salmonella* cells with and without fully modified PhoPQ modified LPS by ethidium bromide assays, and monolayers of extracted LPS formed at the air-water interface that are either fully modified through the *PhoPQ*-controlled processes or not modified at all—hereafter the constituted mutant LPS, $PhoP^c$, and the null mutant LPS, $PhoP^-$, respectively. The monolayers are probed using Langmuir trough isotherms, as well as surface x-ray scattering methods to study their structure and interaction with a large, hydrophobic antibiotic, novobiocin. These data give us molecular-level insights into how these types of drugs permeate through modified outer membranes—the first line of defense for Gram-negative bacteria cells.

MATERIALS AND METHODS

Bacterial strains

The strains used are derivatives of *S. enterica* serovar Typhimurium CS093 (= ATCC 14028). For comparisons between $PhoP^-$ and $PhoP^c$ strains, strains containing phoP102::Tn10d-cam (CS015) and pho-24 (CS022) (9), respectively, were used. To make the LPS more soluble in organic solvents, a *galE* mutation, which removes most of the polysaccharide side chains of LPS, was introduced from strain LT2M135 by P22 transduction and the *galE* transductants were screened on galactose-BTB agar plates.

LPS extraction

LPS were extracted using the phenol/chloroform/petroleum ether extraction procedure described by Galanos et al. (10) followed by acetone precipitation and ethanol washing described by Qureshi (11). Briefly, cells were grown in 50 mL of lysogeny broth (LB) (10 g Bacto-tryptone per liter, 10 g Bacto-yeast per liter, 5 g of NaCl per liter) overnight with shaking at 37°C. This culture was diluted in one liter of fresh LB and culture was grown with shaking at 37°C until the optical density at 600 nm (OD600) reached a value between 1.5 and 1.8. Cells were harvested by centrifugation and washed twice with water, followed by ethanol, acetone, and diethyl ether. LPS was then extracted with a phenol/chloroform/petroleum ether mixture 2:5:8 (v:v:v) and the extract was centrifuged. The supernatant that contained LPS was then placed in a rotary evaporator to remove chloroform and petroleum ether. LPS was precipitated with acetone and diethyl ether and the precipitate was extensively washed with ethanol to remove the remaining phenol. Acid treatment was performed according to Snyder and McIntosh (12) to make certain that LPS contained one defined salt form.

Minimum inhibitory concentrations

Minimum inhibitory concentration (MIC) values correspond to the lowest concentration of drug molecule required to inhibit visible growth of microorganisms after overnight incubation. MIC values were determined by the gradient diffusion plate method as described previously (9).

Ethidium bromide influx

Ethidium bromide assays were performed following the procedure described by Murata et al. (9). Ethidium bromide was added to 6 μM, and its influx into cells was determined at room temperature with excitation and emission wavelengths of 545 and 600 nm, respectively. Carbonyl cyanide 3-chorophenylhydrazone (CCCP) was added in some experiments at a final concentration of 25 μM.

Langmuir monolayers

Langmuir monolayers were obtained by spreading chloroform solutions of LPS over an aqueous subphase of 20 mM HEPES buffer, pH 7.0 containing either 0–20 mM Mg^{2+} or10 mM EDTA, and 90 mM NaCl. MilliQ-Plus water with resistivity 18.2 MΩcm (pH 5.5) was used for preparing buffer solutions. The π-A isotherms were evaluated in a mini-KSV (Biolin Scientific, Stockholm, Sweden) Langmuir trough, previously calibrated using MilliQ-Plus water with a surface tension of ~72.4 mN m^{-1}. The trough was equipped with a surface pressure sensor (Wilhelmy method). π-A isotherms were recorded on monolayer compression using movable barriers with a speed of 10 $Å^2$ $molecule^{-1}$ min^{-1}. Initially, a Langmuir trough with total capacity of 250 mL was filled with buffer solution, and then LPS was spread on the air-water interface and 20 min elapsed for solvent evaporation. All the experiments were performed at 22 $\pm$ 1°C.

X-ray specular reflectivity and grazing incidence x-ray diffraction

X-ray specular reflectivity (XR) elucidates the structure of the Langmuir monolayers of LPS by Fourier inversion of the normalized reflectivity data to yield the layer's electron density (ED), normal to the interface, as previously described (13). All x-ray experiments were done in triplicate, and were found to be fully reproducible. Data obtained were fit by both model-independent (MI) and model-dependent (MD) methodologies via StochFit (14) and RFit2000 (15), respectively, until solutions were found to be in good agreement. Modeling of electron densities from reflectivity curves is done as a process, which iterates between complex models of both b-spline interpolation and Stochastic tunneling a model of three boxes per angstrom (Å) of variable (ED) through the reflectivity curves, resulting in a continuous curve of ED, which represents the absolute chi-squared minima in the parameter space. The fitting of the ED curves follows agreement between MI curves to a 1–3 box model with roughnesses, which minimizes a chi-squared value between a purely hypothetical ED model, and the generated MI ED curves. Values minimizing this fit are then used as an initial model, which is fit to the reflectivity data using the Parratt

formalism of discrete boxes of density convolved by roughness—or error functions—corresponding the regional smearing due to thermal capillary fluctuations on the order of 2.7 Å. Parameter variations fit to values of thickness, density, absorption, and roughness with limits imposed by ab initio molecular conditions. Final parameters used in MD curves represent these fits in which no calculated uncertainty were allowed to exceed 20%, and most reported are between 1% and 3%. Calculations done concerning numbers of electrons are in good agreement between all models. Drug/lipid ratios are calculated by summing the electron densities multiplied by the average area per molecule, with 50% of excess electrons in the headgroup being attributed to water, as previously detailed (16).

Grazing incidence x-ray diffraction (GIXD) provides details about the in-plane, lateral order of the constituent molecules' patterning via diffraction from the hydrophobic tails, and is an ideal tool for elucidating changes in the order at the interface (13,17,18). Diffraction peaks were fit and analyzed in OriginPro by fitting the intensity peaks—less their linear background to a single Lorentz-Gauss (1:1) crossed peak. All x-ray experiments were carried out at Argonne National Laboratory's Advanced Photon Source in sector 9-IDC with incident light of wavelength $\lambda = 0.920175$ (Å) and a photon energy of $E = 13.474$ keV. The custom-built Langmuir trough was mounted in a He-filled, sealed canister and equipped with a moveable single barrier. The surface pressure was monitored using a Wilhelmy plate and held at a constant value of 30 mN m^{-1} corresponding to the most realistic molecular packing of LPS molecules in vivo. Constant-pressure insertion experiments were performed at a fixed temperature of 22 ± 0.2°C and allowed ~60 min to reach equilibrium. XR measurements were carried out over the range of angles corresponding to Q_z values of ~0.01–0.78 $Å^{-1}$, where $Q_z = (4\pi/\lambda)\sin(\alpha)$; λ is the wavelength and α is the identical incident and reflected angles. GIXD measurements were performed by setting a fixed α angle at 0.85% of the surface critical ($Q_z = 0.0217$ $Å^{-1}$) and sweeping the detector arm through a set of angles, 2θ, such that $Q_{xy} = (2\pi/\lambda)\sin(2\theta/2)$, around the trough center. GIXD peaks were subject to linear background subtraction and fit as single Lorentz-Gauss peaks. Diffraction peaks give the d-spacing of the hydrocarbon tails, such that the peak location relates to the spacing by $d = 2\pi/Q_{xy}$, and the coherence length is given by the Sherrer formula, $L_{coherence} = 0.9^* (2\pi/\lambda)^* (1/\xi)$, where ξ is the intrinsic full width half-maxima of the fit peak, or $(FWHM^2 - \Delta^2)^{1/2}$ and Δ is the resolution of the Soller slits. Errors in Qxy are given by the acceptance of the Soller slits, fixed at 1.4 milliradians (9.56×10^{-3} $Å^{-1}$).

RESULTS

The experimental system

We started from *S. enterica* sv. Typhimurium strains CS015 and CS022,9 in which the PhoPQ regulation is either totally absent due to the deletion of the *phoP* gene, or fully active due to the constitutive expression of the PhoPQ system, respectively. The lipid A moieties of the LPS from these strains are known to have the structures shown in Fig. 1, based on GC-MS studies (19).

LPS containing the long carbohydrate chains cannot be dissolved in organic solvents, and thus could not be spread on the air-water interface. We used LPS (often called Rc-chemotype) from *galE* mutants, which contains all of the basal core sugar residues (heptose and KDO) as well as one of the R core sugars (glucose) but lack the O chain and most of the R core (Fig. 1), yet produce an essentially unaltered permeability barrier (6). We first ascertained that the permeability properties of PhoPQ-constitutive and PhoP-deletion strains are similar to those strains producing LPS containing the full carbohydrate chains, earlier studied by Murata and others (9).

Remodeling of lipid A produces a more robust permeability barrier also in *galE* background

Murata et al. (9) observed a twofold decrease in susceptibility to novobiocin for PhoP-constitutive (hereafter called $PhoP^c$) strain in comparison with PhoP-null (hereafter called $PhoP^-$) strain. In our strains that expressed the constitutive levels of AcrAB-TolC efflux pump (20) the levels of MIC were higher in comparison with the strains used by Murata et al. (9) that lacked this major efflux pump, yet similar differences in susceptibility were found, with MIC values of 40 and 14 μg mL^{-1} for $PhoP^c$ and $PhoP^-$ strains, respectively. These results indicate that the difference in the permeability of the LPS leaflet is still found in the presence of *galE* mutation.

Influx of ethidium was examined to determine the permeability of the LPS leaflet in intact *Salmonella* cells. Ethidium is a large, hydrophobic and positively charged dye, and it appears to penetrate exclusively across the LPS/phospholipid asymmetric bilayer of the OM from mutant studies (6). Ethidium produces a fluorescent signal when bound to nucleic acids inside the cells.

In the presence of CCCP, which inactivates the *AcrB* efflux pump, the outer membrane permeability of the CS015 *galE* strain ($PhoP^-$) was much higher than that of CS022 *galE* strain ($PhoP^c$) (Fig. 2). In the absence of CCCP, the presence of active efflux apparently enhanced the differences in ethidium influx rates. These data indicated that the remodeling of lipid A in $PhoP^c$ resulted in a more robust barrier to the permeation of novobiocin and ethidium.

Langmuir monolayer studies

To better examine these differences at the molecular level, LPS from the *galE* derivatives of CS015 and CS022 were extracted and reconstituted as Langmuir monolayers (Fig. 3, *A* and *B*). Building these nanostructured thin films at the air-buffer interface allows us to evaluate lateral interactions to explain the permeability results. The limiting area for a $PhoP^-$ LPS molecule, calculated from the tangent of the curve immediately before the collapse, was ~130 $Å^2$, which can be compared with some values reported in the literature for LPS preparations from related species (21,22). Brandenburg and Seydel (21) obtained data for limiting the area of LPS from different *Salmonella minnesota* mutants ranging from 105 to 125 $Å^2$. Le Brun et al. (22) showed that the tails of Rc LPS from a rough strain of *Escherichia coli* occupied a total area of 109 $Å^2$ with a tilt angle from the surface normal between 15° and 29°. In contrast, for $PhoP^c$ LPS, the limiting area was 175 $Å^2$. Presumably, this ~45 $Å^2$ increase was caused by the molecular areas contributed by the extra palmitoyl chain in the apolar

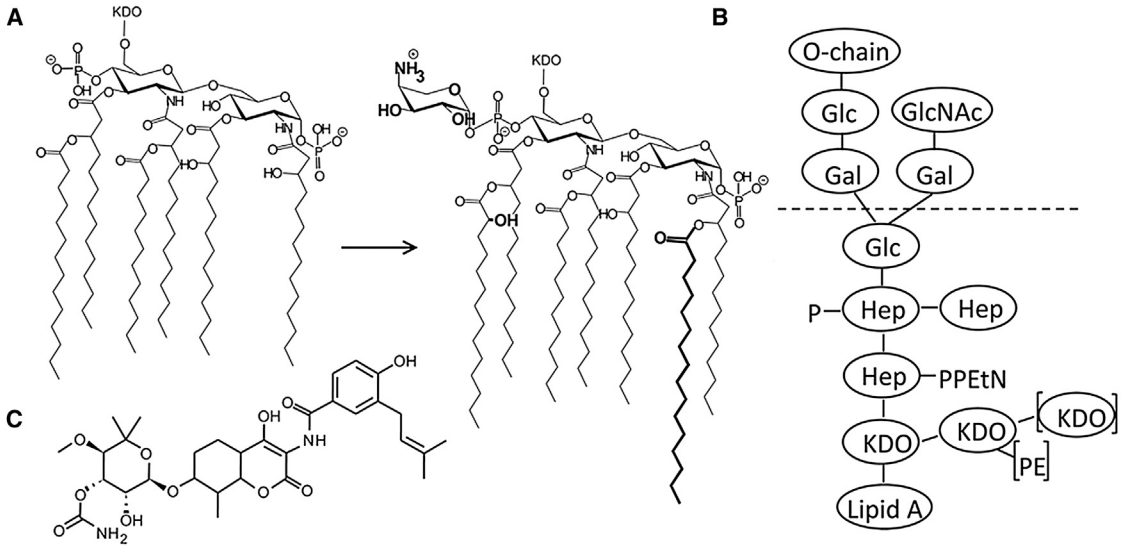

FIGURE 1 Structure of LPS. (*A*) Modification of lipid A structure by the *PhoPQ* regulatory system, with the additional features of the modified lipid A in bold letters. (*B*) The structure of the LPS in *S. enterica*, emphasizing the structure of the carbohydrate portion. The *galE* strains used lack the portions above the dotted lines. Moieties in brackets are not present in stoichiometric amounts. Abbreviations: Glc, glucose; GlcNAc, *N*-acetylglucosamine; Gal, galactose; Hep, heptose; KDO, 2-keto-3-deoxyoctulosonic acid; PE, phosphoethanolamine; PPEtN, pyrophosphoethanolamine. (*C*) The structure of novobiocin.

region, and the aminoarabinose residue in the polar region of this LPS.

Compressional modulus (Cs^{-1}) for the isotherms were calculated as defined by Davies and Rideal (23), –A $(\partial\pi/\partial A)T$. Even though Cs^{-1} values in both phoP null and $phoP^c$ indicated that monolayers were in the liquid-expanded two-dimensional phase, $phoP^c$ presented higher values of Cs^{-1} all over the compression curve, compared to phoP null. For example, at 30 mN m^{-1}, which is widely accepted as a monolayer surface pressure yielding lipid packing with molecular areas most accurately corresponding to those in biological membranes, 15 Cs^{-1} for 16.5 mN m^{-1} and for $PhoP^c$ LPS this value was 31 mN m^{-1}, indicating that the latter is less easily compressible. Measurements of Langmuir isotherms were also carried out with varying concentrations of Mg^{2+}. Isotherms done on the differing suphases showed no significant changes, thus no ions were used in further experiments.

XR and diffraction analysis of LPS monolayers

XR (24) was used to analyze ED distributions of LPS monolayers in the direction perpendicular to the monolayer surface (Table 1; Fig. 3 *B*). The LPS from $PhoP^-$ and $PhoP^c$ strains were found to have an overall thickness of 32.3 Å and 39.4 Å, respectively, which were best described by three distinct regions, or boxes. Each box corresponds to a region of constant ED adjoined together by a normal curve, which describes the roughness between each region; each normal curve adjoining regions is <4 Å in all cases mentioned. Known structures of individual LPS molecules point to three major regions corresponding to each box: a set of hydrophobic tails aligned toward the air, a diphosphoryl headgroup containing the diglucosamine group and possibly the KDO residues, and the outer head region containing the Glc and Hep residues.

$PhoP^-$ LPS had a tail region 13 Å long, a head region also 13 Å long, and an outer core of 6.2 Å (Table 1). The ED of these regions was comparable to the known density of water (0.334 e^- $Å^{-3}$). The lower density of the tail region corresponds with previous studies of lipid compounds at the air-water interface (16,25,26). Density and length of the headgroup would indicate the presence of the diphosphoryl diglucosamine and possibly an additional set of sugars, the KDOs. The final region is composed of the outermost sugars, such as one glucose and three heptose residues, with the corresponding length of 6 Å. When GIXD analysis (13,18) was used to measure hydrocarbon chain spacing (Table 2), it could be best described by a single spacing visualized as ideal hexagonal packing between identical cylinders, or a distorted rectangular unit lattice, where each unit cell corresponds to a single hydrocarbon chain within a crystalline domain upon the surface. Spacing between the hydrocarbon tails for the $PhoP^-$ LPS was 4.16Å, with average crystalline patch diameters (given by the correlation length) of 215 Å.

The $PhoP^c$ LPS could also be modeled as a three-region molecule at the interface with an overall length of 39.4 Å. A lipid tail region had a slightly longer length of 14.7 Å, and the ED was ~10% higher than in $PhoP^-$ LPS. These changes probably reflect the presence of an additional palmitoyl group in the $PhoP^c$ LPS. The $PhoP^c$ LPS headgroup had an increased depth of 15.3 Å, caused by the addition of an aminoarabinose to this group and the addition of a

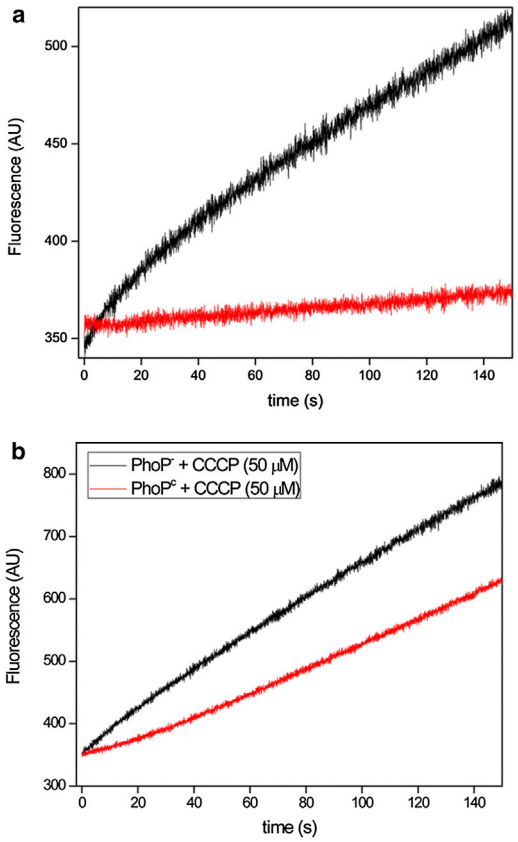

FIGURE 2 Ethidium influx into CS015 *galE* (phoP^{-}) (*black*) and CS022 *galE* (phoP^{c}) (*red*) cells in the absence (*a*) and presence of 25 μM CCCP (*b*). To see this figure in color, go online.

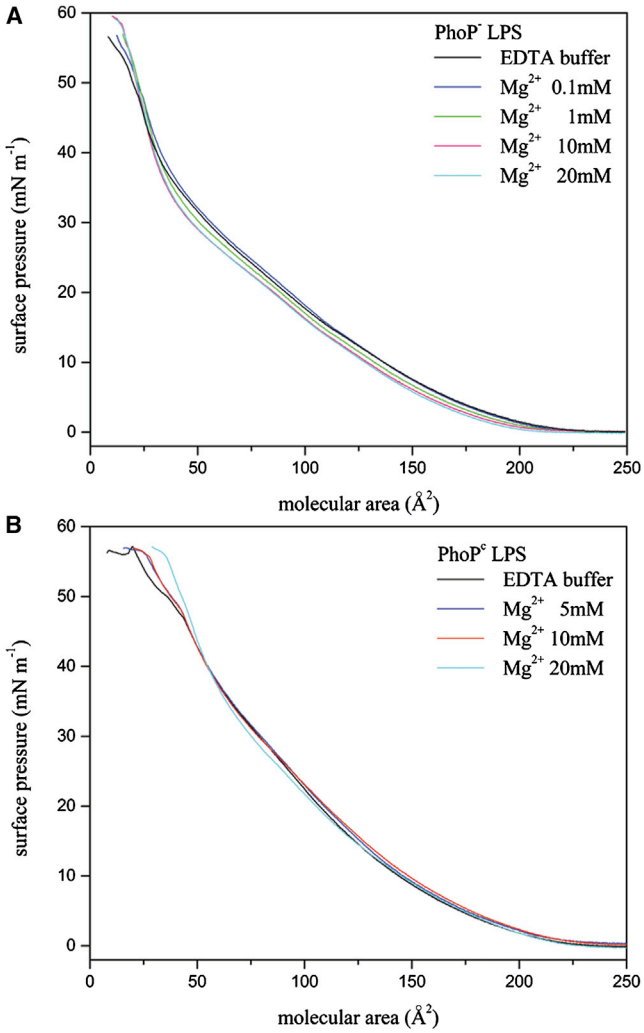

FIGURE 3 Langmuir isotherms for PhoP^{-} (*A*), and PhoPc (*B*) LPS either in the presence of EDTA or varying levels of magnesium in the subphase. To see this figure in color, go online.

2-hydroxy group very close to it. Headgroup density was found to be 0.40 e^{-}Å^{-3}, which is slightly higher than that of PhoP^{-}, a surprising result. The outer headgroup had an increased depth of 9.3 Å; this was somewhat unexpected, but is likely to reflect the presence of additional components in other regions, which would allow the sugars to move more deeply into water. Diffraction of the PhoP^{c} LPS tails showed a similar packing with average d-spacing between tails found to be 4.23Å, a value is only slightly larger than that in PhoP^{-} LPS. However, coherence length was ~165 Å, also a smaller value than that seen in PhoP^{-} LPS, but with much higher intensity, pointing to a larger number of diffracting domains of smaller individual size. This suggests that PhoP^{c} LPS tends to form a more stable collective assembly than the PhoP^{-} LPS.

The effects of novobiocin

Novobiocin was introduced into the subphase bringing the system to a final concentration of 14 μg mL^{-1}, which corresponds to the determined MIC value of novobiocin against the PhoP^{-} mutant. Comparison of the XR-derived ED profiles before and after drug treatment is shown in Fig. 3 *B*. Black curves correspond to the model-independent fit of the data before drug treatment, and red ones to those after drug addition. The total film area did not change after the introduction of the drug in either the PhoP^{-} or PhoP^{c} LPS. With PhoP^{-} LPS, novobiocin affected all regions of LPS, resulting in a significant increase in ED and a slight increase in the overall length of the layer (Fig. 3 *B*, Table 1). The most prominent change was that two, rather than three regions now best described the model, distinct regions, with the head and sugars regions of the previously drug-free LPS fused into a single region. The new, to our knowledge, structure showed a shortened tail region with an increased density, caused by the presence of drug molecules between hydrocarbon chains. The disappearance of the border between the head and sugars regions is also caused by the presence of drug molecules in these areas (see below), corroborated by the increased ED in these regions (Table 1).

XR studies before and after introduction of novobiocin allowed direct measurement of the total drug content present

TABLE 1 Size and electron density in the three layers of the LPS monolayer from XR data fitted by MD fitting using RFIT2000

LPS and Drug Added	Depth (Å) (Top) and Electron Density (e^-/Å^3) (Bottom)			
	Tail	Inner Head Group	Outer Head Group	Total
PhoP-null	13.04	13.04	6.21	32.29
	0.29	0.37	0.36	
PhoP-null + Nov	10.66	22.78[a]		33.44
	0.32	0.40[a]		
PhoP-const	14.76	15.31	9.36	39.43
	0.31	0.40	0.36	
PhoP-const + Nov	15.13	14.22	11.36	40.72
	0.29	0.42	0.38	

[a]These two regions were best modeled as a single slab in this case.

in the LPS. Drug/lipid ratios are calculated by counting the number of electrons in the average molecular volume before and after the drug was introduced, and accounting that each head region is assigned a 50% hydration at the given molecular area, found from a Langmuir isotherm (16). The number of electrons in the novobiocin molecule (324 electrons) is then used to account for excess density, presented as the shaded regions in Fig. 4 *B*. There was no observed change in the film's area or surface pressure after injection of the drug; all extra electrons can be attributed to the presence of drug within the layer. A Drug/-lipid molar ratio of the PhoP$^-$ LPS/novobiocin structure was 0.79; novobiocin appeared to be present in all areas of the layer as judged by the increased ED (Fig. 4 *B*), with the highest concentration within the head and sugars regions. Novobiocin molecules are included in the cartoon models of molecular structure (Fig. 4 *C*).

Introduction of novobiocin into the system is reflected by a marked change in the diffraction of the hydrocarbon tails for the PhoP$^-$ mutant, seen in the GIXD experiment (Fig. 5; Table 2). Although the spacing of the tails remained essentially the same, a large difference was observed in the change in crystallite coherence, the coherence length leaping from 215 Å to $\geq$591 Å upon insertion of the drug in the diffracting parts of the layer (Table 2). Order is typically destroyed by the introduction of agents within a monolayer (18,27,28), but this drug had the effect of strongly increasing the size of the ordered regions in the layer.

In contrast to the PhoP$^-$ LPS, PhoP^c LPS showed a much milder reaction to the novobiocin addition (Fig. 4; Table 1). Layer thickness of the LPS displayed a slight increase of 1.3 Å, but could still be fit into three distinct regions as before. The most noticeable change in length occurred in the sugars region in PhoP^c LPS, which saw an increase of 2 Å, whereas the headgroup saw a loss of 1 Å; and the ED in these regions showed only a slight (5%) increase; these changes reflect the presence of drug molecules in the hydrophilic region. The length of the tails region experienced only minimal changes, and the ED here actually decreased upon addition of novobiocin (Fig. 4 *B*; Table 1), suggesting the absence of the drug molecule in the hydrophobic region. The overall Drug/lipid ratio—as described previously—of this layer was 0.29; most of the drug molecules were located in the outer sugar groups of the LPS (Fig. 4 *C*). Addition of novobiocin to PhoP^c LPS caused no change in the hydrocarbon tail spacing (Fig. 5) as seen in PhoP$^-$, but an increase in the crystalline coherence length from 165 Å to 257 Å, an effect also observed in the PhoP$^-$ mutant.

DISCUSSION

Human pathogens are required to survive under different environmental conditions through their life cycle. *S. enterica* sv. Typhimurium, for example, must live in the presence of several mM concentrations of bivalent cations in our intestinal tract, and after capture by phagocytosis must also survive in the phagosomes that are rich in cationic antimicrobial peptides (29). One important mechanism that allows this adaptation to vastly different environmental conditions is thought to be the modification of LPS molecules on the cell surface by the *PhoPQ* two-component regulatory system. Recognizing the presence of cationic peptides within phagosomes (8), the activated *PhoPQ* system produces three alterations in the lipid A portion of LPS, the addition of aminoarabinose, a palmitoyl chain, and a 2-OH group to one of the fatty acyl chains (Fig. 1 *A*) (19). The addition of aminoarabinose decreases the electrostatic repulsion between the neighboring, polyanionic, lipid A moieties; the addition of one more hydrocarbon chain by the palmitoyl transferase *PagP* also stabilizes the LPS leaflet by increasing the hydrophobic interaction between the neighboring lipid A; addition of a 2-hydroxyl group increases the hydrogen bonding between neighboring LPS. All three modifications are expected to result in the stabilization of LPS leaflet or monolayer. Indeed, the

TABLE 2 Lateral crystallinity of LPS films given by GIXD data

Sample	Position of Q_{xy} Maxima (Å^{-1})	FWHM	*d*-Spacing (Å)	L_{coh} (Å)	Lattice Spacing (Å)[a]	A_{uc} (Å^2)[b]
PhoP$^-$	1.51	0.028	4.16	215.7	4.80	19.95
PhoP$^-$ +Nov	1.52	0.008	4.14	591.6	4.78	19.80
PhoP^c	1.49	0.036	4.23	165.4	4.88	20.62
PhoP^c +Nov	1.49	0.024	4.23	256.9	4.88	20.62

FWHM, full width half-maximum width half maximum; L_{coh}, lateral coherence length.
[a]Spacing between diffracting planes in the monolayer.
[b]A_{uc} is the derived area per unit cell corresponding to a single hydrocarbon chain.

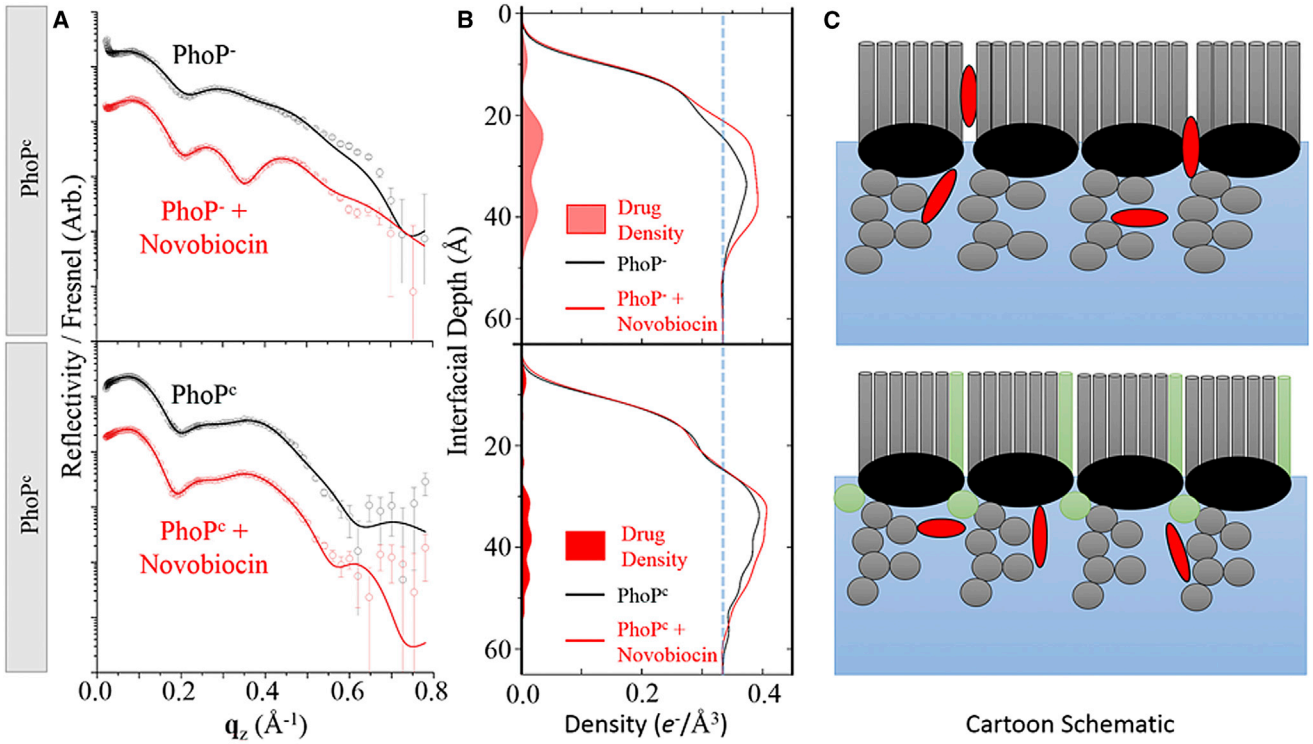

FIGURE 4 (*A*) Reflectivity data (*symbols*) and best fits (*lines*) generated using RFIT2000 corresponding to a MD Parratt regime of 2–3 boxes of fixed density convolved by Gaussian roughness between boxes. Reflectivity is plotted, as usual, against the scattering vector Q, which is equal to $4\pi \sin(\alpha)/\lambda$, where α and λ denote the angle of incidence and the wavelength of the x-ray. Q therefore has a unit of $Å^{-1}$, and is in the direction perpendicular to the plane of the monolayer, thus Q_z. (*B*) Derived ED normal to the interfacial surface. MD ED curves generated by simulated annealing in StochFit before and after drug insertion are displayed as black and red curves, respectively. (*C*) Cartoon schematics of the LPS layers' equilibrium distributions after introduction of novobiocin, where alterations of the electron densities of LPS in the cartoon are highlighted in green, the drug in red, and the lipid regions in gray/black. To see this figure in color, go online.

PhoPQ-induced modifications are known to make *Salmonella* cells more resistant to not only cationic antimicrobial peptides (30–32) but also to a number of large, lipophilic antimicrobial agents (9).

We characterized the physical properties of the *PhoPQ*-modified and unmodified LPS, after confirming the difference in permeability in strains containing *galE* mutation, which truncated the carbohydrate chains of LPS (Fig. 1). The monolayer studies by Langmuir isotherms (Fig. 3) and x-ray scattering techniques (Figs. 4 and 5), showed not only that the modified LPS occupied a larger area as expected (Figs. 4 and 5), but also had a slightly more extensive long-range organization (Table 2), confirming the notion that the modification helps in stabilizing the two-dimensional assembly of LPS molecules. An important observation was that a lipophilic antibiotic, novobiocin, when added to the aqueous subphase and allowed to equilibrate with the LPS monolayer, was able to penetrate through the headgroup region and partitioned into the hydrocarbon region in the monolayer of the unmodified LPS. Penetration was prevented in *PhoPQ*-modified LPS (Fig. 4, *B* and *C*). The total film area in both cases remained constant. Furthermore, the presence of novobiocin within the tails of the null mutant resulted in a shift in diffraction to a higher Q. No such shift was detected in the modified LPS, likely because of the drug's inability to penetrate into the hydrocarbon chains. These findings correlate well with the increased novobiocin MIC value seen in intact cells of the $PhoP^c$ strain, 40 $\mu g\ mL^{-1}$, instead of 14 $\mu g\ mL^{-1}$ in the $PhoP^-$ strain. Modification of LPS by the *PhoPQ* regulation system seems to explain the increase in novobiocin resistance.

It was observed that novobiacin makes LPS molecules pack tighter, and that it inserts into the tail region of the unmodified LPS. Taken together, this indicates the hydrophobic nature of the interactions between the novobiocin and the LPS. The additional palmitoyl appended by the *PhoPQ* system allows the mutant LPS to pack into more crystalline domains, (evident by the increased scattering intensity seen in GIXD measurements in Fig. 5), and, likely, be the key reason for novobiocin not being able to associate with the LPS lipid tails in the constituted mutant. Alterations of the LPS headgroups with a positively charged aminoarabinose alters the electrostatics between the drug and LPS, while also making the LPS associate together into more crystalline domains. The addition of a single positive charge to the headgroup lowers the coulomb barrier between the adjacent

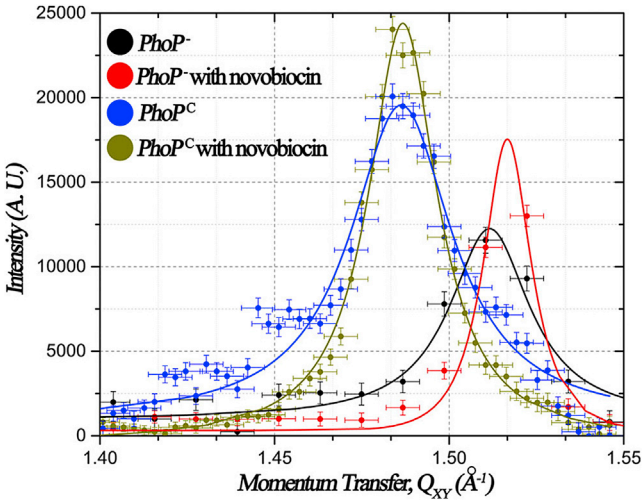

FIGURE 5 Grazing incidence x-ray diffraction data (*symbols*) and corresponding Lorentz-Gauss (1:1) fits generated by OriginPro (*lines*) after linear background subtraction. Diffraction intensity is plotted against the scattering vector Q as in Fig. 4, but in the direction of the plane of the monolayer, thus Q_{xy} rather than Q_z. Errors in Q_{xy} given by the resolution of the Soller collimator given at 1.4 mrad, or 9.56×10^{-3} Å^{-1} at the fixed energy of 13.4737 keV with a $\Delta E/E \sim 10^{-4}$. To see this figure in color, go online.

polyanionic molecules. As the outer and then the inner heads are the first points of contact for the drug molecule, the changes in this region must therefore govern the initial LPS-drug interaction. We suggest that the drugs initially accumulate in the outer headgroups and tangle with the outer sugars, forcing the LPS molecules to more closely associate. This association is then marked by sharpening of the LPS diffraction peaks, which equates as the size of the crystalline domains growing on the surface. As the crystalline fraction of the membrane increases, the disordered regions have an increasing area available per molecule, which will eventually allow for the accommodation of drug molecules. This behavior is corroborated by the larger compression modulus of the PhoP^c LPS; the additional tail makes the film much more difficult to compress or accommodate drug molecules as the LPS is corralled into larger crystallites.

Based on our experimental data alone, we cannot claim sufficient mechanistic evidence of how the penetration of novobiocin drugs is prevented by the *PhoPQ*-regulated modification of all LPS. Our original hypothesis of increased lateral interaction between neighboring PhoP^c LPS molecules remains neither supported nor rejected. However, the crystalline domain of PhoP$^-$ LPS shows a dramatic increase in the presence of novobiocin, it becomes tempting to speculate that this might create high permeability, possibly by the resultant increases in the area occupied by the unordered domain. In such a way, the novobiocin is increasing the size of the crystallites in the monolayer, directly seen by the thinning of the Bragg peaks in the diffraction signal (Fig. 5). Furthermore, the peak intensity and integral intensity of the diffracted signals increases in both cases after drug treatment, though most obviously for the PhoP^c LPS. Such observations further support the possibility of crystalline growth being responsible for novobiocin penetration through the LPS onto the drugs known cytoplasmic targets. More experimentation is needed to evaluate this hypothesis as the mechanism responsible for more general drug permeation through the outer membrane.

It should be mentioned that LPS monolayers have been studied earlier by similar approaches. LPS of somewhat more extended carbohydrate chain (Ra-type) was used to examine the interaction with a 20-residue, highly cationic peptide PA19-2.5 (33). This highly hydrophilic molecule was found to penetrate into the headgroup region in the absence of Ca^{2+}, but not in its presence.

CONCLUSION

Our studies were carried out in *S. enterica,* where most of the clinically useful antimicrobial agents rapidly pass through porin channels (1), and thus the diffusion of antibiotics through the LPS/phospholipid bilayer region of the outer membrane is not immediately relevant to public health. However, the most problematic bacterial pathogens now threatening human health because of their extensive multidrug resistance, or pan resistance, are *Pseudomonas aeruginosa* and *Acinetobacter baumannii* (34,35), and both these organisms lack the high permeability nonspecific porins (36,37). Although carbapenems most often use a specific channel OprD (38), in the often-encountered carbapenem-resistant strains the role of penetration through the bilayer region of the outer membrane becomes important, and our current results become quite relevant. Furthermore, polycationic compounds such as polymyxin and colistin are often the only option left for these pan-resistant pathogens (39), and their penetration obviously depends on the interaction with unmodified and modified LPS. We believe that our approaches are important in developing additional effective agents for these problem pathogens in view of these circumstances.

AUTHOR CONTRIBUTIONS

T.M.N., H.N., and D.G. conceived the idea of this study. Biological assays and isotherm measurements were conducted by T.M.N. X-ray scattering experiments were performed by M.W.M. and K.A. Data were analyzed and modeled by M.W.M. X-ray models were interpreted by M.W.M. and D.G. I.K. oversaw the x-ray experiments. H.N. and D.G. supervised the project. M.W.M., T.M.N., H.N., and D.G. wrote the article.

ACKNOWLEDGMENTS

This work was supported by funds from the National Institutes of Health (NIH) (AI009644 to H.N., AI073892 to D.G.), and Defense Advanced Research Projects Agency (DARPA) (W911NF-09-1-378, D.G.). T.M.N. was supported by a fellowship from the Brazilian funding agency

Coordination for the Improvement of Higher Education Personnel (CAPES) (Proc # BEX 4058/11 -9). Use of the Advanced Photon Source (APS) was supported by the U.S. Department of Energy (DOE) under contract No. W-31-109-Eng-38. M.W.M. was supported in part by the Illinois Institute of Technology Dean's fellowship, the National Science Foundation (NSF) fellowship grant under the Adler Planetarium and Astronomy Museum, and Argonne National Laboratory's X-ray science division (XSD), under the inelastic X-ray nuclear scattering group (IXN).

REFERENCES

1. Nikaido, H. 2003. Molecular basis of bacterial outer membrane permeability revisited. *Microbiol. Mol. Biol. Rev.* 67:593–656.
2. Nikaido, H., E. Y. Rosenberg, and J. Foulds. 1983. Porin channels in *Escherichia coli*: studies with beta-lactams in intact cells. *J. Bacteriol.* 153:232–240.
3. Yoshimura, F., and H. Nikaido. 1985. Diffusion of beta-lactam antibiotics through the porin channels of *Escherichia coli* K-12. *Antimicrob. Agents Chemother.* 27:84–92.
4. Plésiat, P., and H. Nikaido. 1992. Outer membranes of gram-negative bacteria are permeable to steroid probes. *Mol. Microbiol.* 6:1323–1333.
5. Plesiat, P., J. R. Aires, …, T. Köhler. 1997. Use of steroids to monitor alterations in the outer membrane of *Pseudomonas aeruginosa*. *J. Bacteriol.* 179:7004–7010.
6. Vaara, M. 1993. Antibiotic-supersusceptible mutants of *Escherichia coli* and *Salmonella typhimurium*. *Antimicrob. Agents Chemother.* 37:2255–2260.
7. Vaara, M. 1992. Agents that increase the permeability of the outer membrane. *Microbiol. Rev.* 56:395–411.
8. Prost, L. R., and S. I. Miller. 2008. The Salmonellae PhoQ sensor: mechanisms of detection of phagosome signals. *Cell. Microbiol.* 10:576–582.
9. Murata, T., W. Tseng, …, H. Nikaido. 2007. PhoPQ-mediated regulation produces a more robust permeability barrier in the outer membrane of *Salmonella enterica* serovar typhimurium. *J. Bacteriol.* 189:7213–7222.
10. Galanos, C., O. Luderitz, and O. Westphal. 1969. A new method for the extraction of R lipopolysaccharides. *Eur. J. Biochem.* 9:245–249.
11. Qureshi, N., K. Takayama, …, C. Fenselau. 1984. Position of ester groups in the lipid-a backbone of lipopolysaccharides obtained from *Salmonella*-Typhimurium. *Rev. Infect. Dis.* 6:576–576.
12. Snyder, D. S., and T. J. McIntosh. 2000. The lipopolysaccharide barrier: correlation of antibiotic susceptibility with antibiotic permeability and fluorescent probe binding kinetics. *Biochemistry.* 39:11777–11787.
13. Kjaer, K., J. Alsnielsen, …, H. Mohwald. 1988. An x-ray-scattering study of lipid monolayers at the air water interface and on solid supports. *Thin Solid Films.* 159:17–28.
14. Danauskas, S. M., D. X. Li, …, K. Y. C. Lee. 2008. Stochastic fitting of specular X-ray reflectivity data using StochFit. *J. Appl. Cryst.* 41:1187–1193.
15. Konovalov, O. V., L. A. Feigin, and B. M. Shchedrin. 1996. Statistical evaluation of the accuracy of structure parameter determination from x-ray and neutron reflectivity data. *Kristallografiya.* 41:640–643.
16. Ivankin, A., I. Kuzmenko, and D. Gidalevitz. 2012. Cholesterol mediates membrane curvature during fusion events. *Phys. Rev. Lett.* 108:238103-1–238103-5.
17. Kjaer, K. 1994. Some simple ideas on x-ray reflection and grazing-incidence diffraction from thin surfactant films. *Physica B.* 198:100–109.
18. Andreev, K., C. Bianchi, …, D. Gidalevitz. 2014. Guanidino groups greatly enhance the action of antimicrobial peptidomimetics against bacterial cytoplasmic membranes. *Biochim. Biophys. Acta.* 1838:2492–2502.
19. Guo, L., K. B. Lim, …, S. I. Miller. 1997. Regulation of lipid A modifications by *Salmonella* typhimurium virulence genes phoP-phoQ. *Science.* 276:250–253.
20. Nikaido, H. 1996. Multidrug efflux pumps of gram-negative bacteria. *J. Bacteriol.* 178:5853–5859.
21. Brandenburg, K., and U. Seydel. 1988. Orientation measurements on membrane systems made from lipopolysaccharides and free lipid A by FT-IR spectroscopy. *Eur. Biophys. J.* 16:83–94.
22. Le Brun, A. P., L. A. Clifton, …, S. A. Holt. 2013. Structural characterization of a model gram-negative bacterial surface using lipopolysaccharides from rough strains of *Escherichia coli*. *Biomacromolecules.* 14:2014–2022.
23. Davies, J. T., and E. K. Rideal. 1961. Interfacial Phenomena. Academic Press, New York.
24. Grundy, M. J., R. M. Richardson, …, R. C. Ward. 1988. X-ray and neutron reflectivity from spread monolayers. *Thin Solid Films.* 159:43–52.
25. Ivankin, A., I. Kuzmenko, and D. Gidalevitz. 2010. Cholesterol-phospholipid interactions: new insights from surface x-ray scattering data. *Phys. Rev. Lett.* 104:108101-1–108101-4.
26. Gidalevitz, D., Y. Ishitsuka, …, K. Y. Lee. 2003. Interaction of antimicrobial peptide protegrin with biomembranes. *Proc. Natl. Acad. Sci. USA.* 100:6302–6307.
27. Neville, F., A. Ivankin, …, D. Gidalevitz. 2010. A comparative study on the interactions of SMAP-29 with lipid monolayers. *Biochim. Biophys. Acta.* 1798:851–860.
28. Neville, F., Y. Ishitsuka, …, D. Gidalevitz. 2008. Protegrin interaction with lipid monolayers: grazing incidence X-ray diffraction and X-ray reflectivity study. *Soft Matter.* 4:1665–1674.
29. Martin-Orozco, N., N. Touret, …, S. Grinstein. 2006. Visualization of vacuolar acidification-induced transcription of genes of pathogens inside macrophages. *Mol. Biol. Cell.* 17:498–510.
30. Nummila, K., I. Kilpeläinen, …, I. M. Helander. 1995. Lipopolysaccharides of polymyxin B-resistant mutants of *Escherichia coli* are extensively substituted by 2-aminoethyl pyrophosphate and contain aminoarabinose in lipid A. *Mol. Microbiol.* 16:271–278.
31. Groisman, E. A., J. Kayser, and F. C. Soncini. 1997. Regulation of polymyxin resistance and adaptation to low-Mg2+ environments. *J. Bacteriol.* 179:7040–7045.
32. Guo, L., K. B. Lim, …, S. I. Miller. 1998. Lipid A acylation and bacterial resistance against vertebrate antimicrobial peptides. *Cell.* 95:189–198.
33. Abuillan, W., E. Schneck, …, M. Tanaka. 2013. Physical interactions of fish protamine and antisepsis peptide drugs with bacterial membranes revealed by combination of specular x-ray reflectivity and grazing-incidence x-ray fluorescence. *Phys. Rev. E Stat. Nonlin. Soft Matter Phys.* 88:012705.
34. Livermore, D. M. 2003. The threat from the pink corner. *Ann. Med.* 35:226–234.
35. Bonomo, R. A., and D. Szabo. 2006. Mechanisms of multidrug resistance in *Acinetobacter* species and *Pseudomonas aeruginosa*. *Clin. Infect. Dis.* 43 (*Suppl 2*):S49–S56.
36. Sugawara, E., E. M. Nestorovich, …, H. Nikaido. 2006. *Pseudomonas aeruginosa* porin OprF exists in two different conformations. *J. Biol. Chem.* 281:16220–16229.
37. Sugawara, E., and H. Nikaido. 2012. OmpA is the principal nonspecific slow porin of *Acinetobacter baumannii*. *J. Bacteriol.* 194:4089–4096.
38. Trias, J., and H. Nikaido. 1990. Outer membrane protein D2 catalyzes facilitated diffusion of carbapenems and penems through the outer membrane of *Pseudomonas aeruginosa*. *Antimicrob. Agents Chemother.* 34:52–57.
39. Neonakis, I. K., D. A. Spandidos, and E. Petinaki. 2011. Confronting multidrug-resistant *Acinetobacter baumannii*: a review. *Int. J. Antimicrob. Agents.* 37:102–109.